LA-UR-15-27787 (Accepted Manuscript)

Solar wind conditions leading to efficient radiation belt electron acceleration: A superposed epoch analysis

Li, W.
Thorne, R.
Bortnik, J.
Baker, D.
Reeves, Geoffrey D.
Kanekal, S.
Spence, H.
Green, J.

To be published in: GEOPHYSICAL RESEARCH LETTERS, Vol.42, iss.17, p.6906-6915, SEP 16 2015.

DOI to publisher's version: 10.1002/2015GL065342

Permalink to record: http://permalink.lanl.gov/object/view?what=info:lanl-repo/lareport/LA-UR-15-27787

Solar Wind Conditions Leading to Efficient Radiation Belt Electron Acceleration: A Superposed Epoch Analysis

Li, W.[1], R. M. Thorne[1], J. Bortnik[1], D. N. Baker[2], G. D. Reeves[3], S. G. Kanekal[4], H. E. Spence[5], and J. C. Green[6]

[1]Department of Atmospheric and Oceanic Sciences, UCLA, Los Angeles, California, USA.

[2]Laboratory for Atmospheric and Space Research, University of Colorado, Boulder, Colorado, USA.

[3]Space Science and Applications Group, Los Alamos National Laboratory, Los Alamos, New Mexico, USA.

[4]NASA Goddard Space Flight Center, Greenbelt, Maryland, USA.

[5]Institute for the Study of Earth, Oceans, and Space, University of New Hampshire, Durham, New Hampshire, USA.

[6]Space Hazard Applications, Colorado, USA.

Corresponding Author: W. Li, 7127 Math Sciences Bldg., 405 Hilgard Ave., Los Angeles, CA, 90095, USA. (moonli@atmos.ucla.edu)

Abstract

Determining preferential solar wind conditions leading to efficient radiation belt electron acceleration is crucial for predicting radiation belt electron dynamics. Using Van Allen Probes electron observations (> 1 MeV) from 2012 to 2015, we identify a number of efficient and inefficient acceleration events separately to perform a superposed epoch

analysis of the corresponding solar wind parameters and geomagnetic indices. By directly comparing efficient and inefficient acceleration events, we clearly show that prolonged southward B_z, high solar wind speed, and low dynamic pressure are critical for electron acceleration to > 1 MeV energies in the heart of the outer radiation belt. We also evaluate chorus wave evolution using the superposed epoch analysis for the identified efficient and inefficient acceleration events and find that chorus wave intensity is much stronger and lasts longer during efficient electron acceleration events, supporting the scenario that chorus waves play a key role in MeV electron acceleration.

1. Introduction

Outer radiation belt electrons often exhibit highly dynamic variations [*Blake et al.,* 1992; *Li et al.,* 1993; *Friedel et al.,* 2002] due to a competition between various loss and acceleration processes [*Reeves et al.,* 2003; *Li et al.,* 2007; *Fok et al.,* 2008*; Albert et al.,* 2009; *Xiao et al.,* 2009; *Turner et al.,* 2014]. The response of different populations of electrons with various energies to the same geomagnetic storm can be distinctly different, since 10s-100s keV electron fluxes are enhanced rapidly in association with substorm injections while the timescale for the dynamic response of MeV electrons is typically much longer (~ day) [e.g., *Li et al.,* 2005; *Meredith et al.,* 2011; *Li et al.,* 2014a; *Turner et al.,* 2014]. In this study, we focus on the analysis of highly-relativistic electron dynamics (> 1 MeV), since these so-called "killer" electrons are known to pose significant risks to operating satellites and can potentially cause satellite anomalies or failure [*Baker,* 1998; *Webb and Allen*, 2004; *Choi et al.,* 2011].

45 It is critical to determine the preferential solar wind conditions leading to MeV
46 electron acceleration, since this is a key step towards predicting their evolution based on
47 preceding solar wind conditions. Important solar wind parameters driving relativistic
48 electron dynamics have been extensively studied in the past few decades. *Paulikas and*
49 *Blake* [1979] and *Baker et al.,* [1979] using geosynchronous electron data found that
50 average electron fluxes correlate positively with corresponding averages of the solar wind
51 velocity. A recent "revisited" study by *Reeves et al.* [2011] using a longer-running data
52 set (1989-2010) from the Los Alamos National Laboratory energetic particle instruments
53 has found a triangle-shaped distribution rather than a linear correlation between solar
54 wind speed and electron fluxes, suggesting that the relationship between radiation belt
55 electron fluxes and solar wind velocity is more complex than previously thought.
56 However, in a multi-event study using the Wind spacecraft data during solar minimum,
57 *Blake et al.* [1997] found that relativistic electron enhancement not only depends on a
58 substantial solar wind speed increases, but also on a southward turning of the
59 interplanetary magnetic field, which is further supported by *Iles et al.* [2002] and
60 *McPherron et al.* [2009]. Southward turning of the interplanetary magnetic field is
61 associated with an increase in the seed electron fluxes from a few tens to a few hundreds
62 keV, and these seed electron populations can subsequently be accelerated to highly
63 relativistic (> 1 MeV) energies [*Baker et al.,* 1998; *Li et al.,* 2012; *Boyd et al.,* 2014;
64 *Jaynes et al.,* 2015]. *Lyatsky and Khazanov* [2008] have examined the relationship
65 between > 2 MeV electron fluxes at geosynchronous orbit and solar wind parameters and
66 found that in addition to the positive correlation with the solar wind speed, relativistic
67 electron fluxes decrease with increasing solar wind density. In a very recent paper by *Kim*

68 *et al.* [2015], they concluded that sustained south-oriented or north-south fluctuating
69 interplanetary magnetic field (IMF) B_z and small solar wind density are crucial for
70 electron enhancements at geosynchronous orbit regardless of geomagnetic storms. In
71 summary, previous studies have demonstrated the potential importance of solar wind
72 velocity, interplanetary magnetic field polarity, and solar wind density. However, many
73 of the previous studies [*Paulikas and Blake,* 1979; *Baker et al.,* 1986; *Li et al.,* 2001,
74 2005; *Lyatsky and Khazanov,* 2008; *Borovsky and Denton,* 2009; *McPherron et al.,* 2009;
75 *Reeves et al.,* 2011; *Kim et al.,* 2015] have evaluated electron fluxes at geosynchronous
76 orbit, which is well beyond the region where the radiation belt electron fluxes typically
77 peak and also include adiabatic changes which may not represent a net change in electron
78 phase space density (PSD). Therefore, a careful examination is needed to further
79 determine the important solar wind parameters relevant to MeV electron acceleration.

80 Regarding the dominant acceleration mechanism of radiation belt electrons to MeV
81 energies, a number of studies have clearly shown that chorus waves are fundamentally
82 important for accelerating seed electrons to highly-relativistic energies through efficient
83 energy diffusion [*Horne and Thorne,* 1998; *Summers et al.,* 2002; *Horne et al.,* 2005; *Tao*
84 *et al.,* 2009; *Reeves et al.,* 2013; *Thorne et al.,* 2013; *Li et al.,* 2014a; *Tu et al.,* 2014]. On
85 the other hand, radial diffusion caused by Ultra Low Frequency (ULF) waves also plays
86 an important role in redistributing electrons depending on the radial gradient of the
87 electron PSD and thus accounts for either acceleration through inward radial diffusion or
88 loss of energetic electrons to the magnetopause through outward radial diffusion [e.g.,
89 *Elkington et al.,* 1999; *Hudson et al.,* 1999; *Mathie and Mann,* 2000; *Perry et al.,* 2005;
90 *Ukhorskiy et al.,* 2009; *Huang et al.,* 2010; *Turner et al.,* 2012]. Therefore, it will be very

interesting to compare the chorus and ULF wave evolution during efficient and inefficient electron acceleration events separately to determine their roles in MeV electron acceleration.

In this study, we focus on evaluating important solar wind conditions leading to efficient electron acceleration in the heart of the outer radiation belt using high-resolution electron measurements from Van Allen Probes, which provide excellent coverage over the core region of the Earth's radiation belts. Through a superposed epoch analysis for a number of efficient and inefficient electron acceleration events separately, we clearly identify the essential solar wind conditions leading to MeV electron acceleration. Furthermore, we also perform a superposed epoch analysis of the global chorus wave activity for the selected efficient and inefficient acceleration events to determine their correlation with MeV electron acceleration.

2. Methodology

2.1. Electron Data Analysis from Van Allen Probes

The twin Van Allen Probes [*Mauk et al.,* 2012] have provided an excellent platform for measuring wave and particle evolution in the heart of the radiation belts (< 6 R_E) since their launch in August 2012. Radiation belt electron evolution is analyzed using the data from the Van Allen Probes Relativistic Electron Proton Telescope (REPT) [*Baker et al.,* 2013; *Spence et al.,* 2013] instrument, which measures electron fluxes from ~ 1.8 MeV to > 10 MeV with fine resolution in energy (8 different channels) and pitch angle (36 bins) and thus enables us to evaluate the true non-adiabatic changes by calculating electron PSD for constant adiabatic invariants, as discussed below.

2.2. Calculation of Chorus Wave Intensity Using POES Electron Measurements

Chorus wave intensity evolution on a global scale is critical to evaluate the overall contribution of chorus waves to radiation belt electron dynamics. In this study, we adopt a novel technique of calculating chorus wave intensity from the ratio of the precipitated and trapped electron fluxes (30-100 keV) measured by multiple POES satellites to construct the evolution of chorus wave intensity on a global scale. This technique has been validated by analyzing a number of conjunction events [*Li et al.,* 2013, 2014b; *de Soria-Santacruz et al.,* 2015] and the details of this technique are described in *Li et al.* [2013] and *Ni et al.* [2014]. The great advantage of this technique is that multiple low-altitude POES satellites with a short orbital period (~100 min) enable us to construct a global dynamic model of chorus wave intensity over a broad region of *L*-shell and MLT for individual events, which cannot be obtained from the limited number of near-equatorially orbiting satellites alone.

3. Case Analysis for Efficient and Inefficient Acceleration Events

Figure 1 shows an example of an efficient electron acceleration event, which occurred during the 8-9 Oct 2012 geomagnetic storm, together with solar wind parameters and geomagnetic indices. SYM-H index exhibited a double dip (Figure 1d) associated with the corresponding disturbances in AL (Figure 1e). During the first dip (06-18 UT on 8 Oct 2012), the solar wind dynamic pressure (Figure 1a) was elevated up to ~8 nPa, the solar wind speed (Figure 1b) remained less than 400 km/s, and the IMF in GSM coordinate (Figure 1c) remained in the southward direction for several hours followed by a northward turning. Electron fluxes (Figures 1f-1h) measured by both Van Allen Probes

A and B were averaged every 3 hours within each 0.2 L bin for various energies (1.8, 3.4, and 5.2 MeV) and exhibited decreases during the first dip. To evaluate the non-adiabatic changes, the electron PSD was calculated for a constant first adiabatic invariant (μ = 3433 MeV/G) and second adiabatic invariant (K = 0.10 $G^{1/2}R_E$) and is shown in Figure 1i as a function of L-shell. For this given μ = 3433 MeV/G, the corresponding electron energy varies from ~ 2−3 MeV at ~ 6 R_E to ~7−8 MeV at ~3 R_E. For the adopted K = 0.10 $G^{1/2}R_E$, the corresponding electron pitch angles change from ~40° to ~90° over the trajectories of Van Allen Probes A and B, which were mostly within 15° of the geomagnetic equator. In each 3-hour bin, we calculated the maximum PSD (PSD_{max}) over 2.5-6 R_E and show it in Figure 1j. PSD_{max} reached a minimum near the end of the first dip and started to increase substantially during the second dip. We defined the zero epoch time when this PSD_{max} reaches a minimum value, as indicated by the vertical magenta line, and used the same definition in the superposed epoch analysis discussed in Section 4. Figure 1k shows chorus wave intensity averaged over all MLT sectors obtained from the POES technique, as mentioned in Section 2.2. During the acceleration interval within the second dip chorus wave intensity was persistently strong for ~16 hours over 3-6 R_E, and when chorus wave intensity became weaker after ~12 UT on 9 Oct 2012, the PSD_{max} was essentially unchanged. These observations support the scenario that chorus waves play a key role in accelerating electrons to the MeV range [*Summers et al.,* 2002; *Horne et al.,* 2005; *Reeves et al.,* 2013; *Thorne et al.,* 2013; *Li et al.,* 2014a; *Tu et al.,* 2014].

Figure 2 shows an inefficient acceleration event, which occurred around 1 Oct 2012, using the same format as Figure 1. In association with the significant increase in the solar wind dynamic pressure (Figure 2a), multi MeV electron fluxes (Figure 2f-2j) exhibited a

158 substantial decrease probably due to the dominant magnetopause shadowing effect, as
159 discussed in detail in *Turner et al.* [2014] for this event. During the recovery phase of the
160 storm, the solar wind dynamic pressure remained at a modest value, the solar wind
161 velocity (Figure 2b) was less than 400 km/s, and the IMF was directed in the northward
162 direction for over 24 hours, leading to extremely weak substorm activities (Figure 2e).
163 Consequently, MeV electron fluxes barely recovered after the dropout and were much
164 smaller than the prestorm value. Chorus wave activity (Figure 2k) was strong in the
165 prestorm period along with the ongoing substorm activities, but was extremely weak in
166 the recovery phase in association with weak substorm activities. Similarly, we defined the
167 zero epoch time when the PSD_{max} reached a minimum (dashed vertical magenta line), and
168 used it in the following superposed epoch analysis discussed in Section 4.

169 **4. Superposed Epoch Analysis for Efficient and Inefficient Acceleration Events**

170 Over the period from 1 October 2012 to 1 April 2015 we identified 16 Efficient
171 Acceleration (EA) and 17 Inefficient Acceleration (IA) events to perform a superposed
172 epoch analysis. We defined an EA (IA) event if the PSD_{max} decreased at least by a factor
173 of 5 within 2 days prior to the zero epoch time and the maximum PSD_{max} within 2 days
174 after the zero epoch time is larger (smaller) than 10^{-8} (10^{-9}) c^3 MeV^{-3} cm^{-3}. We note that
175 we did not limit the event selection to geomagnetic storms but selected the events based
176 on electron PSD_{max} evolution. This definition allows us to identify the clear EA and IA
177 events regardless of the geomagnetic storm size.

178 Figure 3 shows the superposed epoch analysis result for 16 EA events. As shown in
179 Figure 3g, electron PSD_{max} starts to rise at around the zero epoch time, after which the

180 solar wind dynamic pressure (Figure 3a) was mostly < 2 nPa, the solar wind velocity
181 (Figure 3b) was elevated to ~ 500 km/s. The most intriguing feature is the prolonged
182 southward IMF B_z (Figure 3c) present after the zero epoch time lasting longer than 16
183 hours, which is associated with strong disturbances in both SYM-H (Figure 3e) and AL
184 (Figure 3f) and favorable for providing source and seed electron populations together
185 with chorus wave intensification [e.g., *Miyoshi and Kataoka*, 2008; *Li et al.,* 2012].
186 However, just prior to the zero epoch time when the electron PSD decreases, the solar
187 wind dynamic pressure substantially increased up to ~ 8 nPa, the solar wind velocity
188 increased from 350 to ~ 500 km/s, and B_z remained in the southward direction for ~ 12
189 hours. As shown in Figure 3d, the magnetopause location on the subsolar distance (L_{MP})
190 estimated based on the equation in *Shue et al.* [1998] moved inward to L_{MP} ~ 8.5 prior to
191 the zero epoch time, but moved out beyond L_{MP} ~ 10 during the acceleration interval.
192 Both the high solar wind dynamic pressure and southward B_z are favorable for causing
193 electron dropouts [e.g., *Lyatsky and Khazanov,* 2008; *Yuan and Zong,* 2013; *Gao et al.,*
194 2015] probably due to the efficient magnetopause shadowing effect followed by the
195 outward radial diffusion process [*Shprits et al.,* 2006; *Turner et al.,* 2012], which is also
196 shown in the inward movement of L_{MP} from ~11 to ~8.5 prior to the zero epoch time.
197 Chorus wave intensity inferred from the POES technique is averaged over a broad range
198 of MLT sectors and the superposed epoch analysis result for the identified 16 EA events
199 is shown in Figure 3h. The chorus wave intensity is persistently strong within 24 hours
200 after the zero epoch time, when the efficient electron acceleration occurs. Moreover,
201 when chorus becomes weaker after 24 hours, the electron PSD_{max} also increases much
202 more slowly. These features support the scenario that chorus waves play an important

role in accelerating electrons to MeV energies [e.g., *Summers et al.,* 2002; *Horne et al.,* 2005; *Thorne et al.,* 2013]. It is interesting to note that although chorus waves were strong several hours prior to the zero epoch time, the PSD_{max} decreases during this interval probably due to the following reason. Over several hours prior to the zero epoch time, the solar wind dynamic pressure was high and the magnetopause was moved closer to the Earth, which favors the magnetopause shadowing loss to be effective and dominant over the chorus-driven electron acceleration, as discussed above.

A superposed epoch analysis is also performed for 17 IA events and the results are shown in Figure 4. Just after the zero epoch time, the electron PSD_{max} exhibits a very slow recovery (Figure 4g), during which the solar wind dynamic pressure (Figure 4a) was low and the solar wind speed (Figure 4b) was less than 450 km/s. Interestingly, IMF B_z (Figure 4c) remained in the northward direction for over 24 hours after the zero epoch time, which led to very weak disturbances in both SYM-H (Figure 4e) and AL (Figure 4f) together with weak chorus wave intensity (Figure 4h). The magnetopause (Figure 4d) was moved inward to $L_{MP} \sim 8$ in association with the PSD_{max} decrease prior to the zero epoch time, but gradually moved out beyond $L_{MP} \sim 10$ subsequently.

In Figures 5a-5g we directly compare the superposed epoch analysis results of the solar wind conditions and geomagnetic indices during EA (red) and IA (blue) events. The most significant difference is that during EA events the IMF B_z (Figure 5c) was persistently in the southward direction during the acceleration interval in contrast to the northward B_z during IA events. The solar wind velocity (Figure 5b) during EA events is larger than that during IA events, whereas the solar wind dynamic pressure (Figure 5a) during EA and IA events after the zero epoch time is comparable. The movement of the

magnetopause location (Figure 5d) is not distinctly different during EA and IA events, which may also suggest that the loss driven by the magnetopause shadowing effect is likely to be comparable. The disturbances in AL (Figure 5e) and SYM-H (Figure 5f) are larger during EA events compared to those during IA events. Moreover, the chorus wave intensity during EA events (Figure 5h) is apparently much stronger and more persistent than that during IA events (Figure 5i), which again supports that chorus waves are fundamentally important for MeV electron acceleration. Therefore, we clearly demonstrate that the most important solar wind conditions leading to efficient electron acceleration include prolonged southward B_z and high solar wind speed. Although not explicitly shown by comparing EA and IA events, the comparison before and after the zero epoch time of EA events clearly suggests that the low solar wind dynamic pressure is also critical to increase the rate of electron acceleration by locating the magnetopause boundary farther away from the Earth, thus minimizing the loss to the magnetopause. For example, in Figure 3 the IMF B_z remains in the southward direction and the solar wind velocity stays high from several hours prior to the zero epoch time, but PSD_{max} only increases after the zero epoch time when the solar wind dynamic pressure becomes low.

5. Summary and Discussion

In the present paper, we determined the preferential solar wind conditions leading to MeV electron acceleration by performing a superposed epoch analysis for a number of efficient and inefficient electron acceleration events separately using the Van Allen Probes electron data from 1 Oct 2012 to 1 April 2015. Our superposed epoch analysis results clearly show that (1) prolonged southward B_z, (2) high solar wind speed, and (3) low solar wind dynamic pressure are critical to lead to efficient MeV electron

acceleration, and the acceleration is most efficient when all three of these conditions are operating simultaneously. We also evaluated the chorus wave evolution using the POES technique [*Li et al.,* 2013; *Ni et al.,* 2014] during efficient and inefficient acceleration events and found that chorus wave intensity is much stronger and lasts longer over a broad region during efficient acceleration events. This is consistent with the scenario that chorus waves play an essential role in MeV radiation belt electron acceleration.

This analysis has been performed using the 2.5 years of Van Allen Probes data from 1 Oct 2012 to 1 April 2015, which is near the solar maximum of the Cycle 24. Although the data coverage is limited, the Van Allen Probes electron data enable us to evaluate the non-adiabatic changes in MeV electron evolution over a broad region of the outer radiation belt (not limited to the geosynchronous orbit) due to the high-quality electron measurements with fine resolution in both energy and pitch angle. Furthermore, low-altitude electron measurements made by multiple POES satellites provide the global distribution of chorus wave intensity in an event-specific perspective, which cannot be obtained by statistical results or direct wave measurements made by near-equatorially orbiting satellites alone.

Since we have identified the most important solar wind conditions leading to efficient electron acceleration, it will be interesting to use the combination of these parameters to test and further predict the spatiotemporal evolution of the highly-relativistic electrons over the entire outer radiation belt. However, this is beyond the scope of the present study and is left for future investigation.

Acknowledgement

This work was supported by JHU/APL contracts 967399 and 921647 under NASA's prime contract NAS5-01072. The analysis at UCLA was supported by the ECT sub-award 13-041, NASA grants NNX11AD75G, NNX14AN85G, NNX11AR64G, and NNX13AI61G, and the Air Force Young Investigator program. We acknowledge the Van Allen Probes data from the REPT and MagEIS instruments obtained from http://www.rbsp-ect.lanl.gov/data_pub/. We greatly appreciate the NOAA POES data obtained from http://satdat.ngdc.noaa.gov/sem/poes/data/ and the NOAA POES team for providing helpful advice. We also thank the World Data Center for Geomagnetism, Kyoto for providing SYM-H and AL index (http://wdc.kugi.kyoto-u.ac.jp/aeasy/index.html), and the Space Physics Data Facility at the NASA Goddard Space Flight Center for providing the OMNI2 data (ftp://spdf.gsfc.nasa.gov/pub/data/omni/omni_cdaweb/).

References

Albert, J. M., N. P. Meredith, and R. B. Horne (2009), Three-dimensional diffusion simulation of outer radiation belt electrons during the 9 October 1990 magnetic storm, J. Geophys. Res.,114, A09214, doi:10.1029/2009JA014336.

Baker, D. N., Higbie, P. R., Belian, R. D. and Hones, E. W. (1979), Do Jovian electrons influence the terrestrial outer radiation zone?. Geophys. Res. Lett., 6: 531–534. doi:10.1029/GL006i006p00531.

293 Baker, D. N., J. B. Blake, R. W. Klebesadel, and P. R. Higbie (1986), Highly relativistic
294 electrons in the Earth';s outer magnetosphere: 1. Lifetimes and temporal history
295 1979–1984, J. Geophys. Res., 91(A4), 4265–4276, doi:10.1029/JA091iA04p04265.
296 Baker, D. N. (1998), What is space weather, *Adv. Space Res.*, 22, 7–16.
297 Baker, D., X. Li, J. Blake, and S. Kanekal (1998), Strong electron acceleration in the
298 Earth's magnetosphere, *Adv. Space Res.*, 21(4), 609–613, doi:10.1016/S0273-
299 1177(97)00970-8.
300 Baker, D. N., et al. (2013), The Relativistic Electron-Proton Telescope (REPT)
301 instrument on board the Radiation Belt Storm Probes (RBSP) spacecraft:
302 Characterization of Earth's radiation belt high-energy particle populations, *Space Sci.*
303 *Rev.*, *179*, 337–381, doi:10.1007/s11214-012-9950-9.
304 Blake, J. B., W. A. Kolasinski, R. W. Fillius, and E. G. Mullen (1992), Injection of
305 electrons and protons with energies of tens of MeV into $L < 3$ on March 24,
306 1991, *Geophys. Res. Lett.*, 19, 821–824, doi:10.1029/92GL00624.
307 Blake, J. B., D. N. Baker, N. Turner, K. W. Ogilvie, and R. P.
308 Lepping (1997), Correlation of changes in the outer-zone relativistic-electron
309 population with upstream solar wind and magnetic field measurements, *Geophys.*
310 *Res. Lett.*, 24, 927–930.
311 Borovsky, J. E., and M. H. Denton (2009), Relativistic-electron dropouts and recovery: A
312 superposed epoch study of the magnetosphere and the solar wind, J. Geophys.
313 Res., 114, A02201, doi:10.1029/2008JA013128.
314 Boyd, A. J., H. E. Spence, S. G. Claudepierre, J. F. Fennell, J. B. Blake, D. N. Baker, G.
315 D. Reeves, and D. L. Turner (2014), Quantifying the radiation belt seed population in

316 the March 17, 2013 electron acceleration event, Geophys. Res. Lett., 41, 2275–2281,
317 doi:10.1002/2014GL059626.
318 Choi, H.-S., J. Lee, K.-S. Cho, Y.-S. Kwak, I.-H. Cho, Y.-D. Park, Y.-H. Kim, D. N.
319 Baker, G. D. Reeves, and D.-K. Lee (2011), Analysis of GEO spacecraft anomalies:
320 Space weather relationships, Space Weather, 9, S06001,
321 doi:10.1029/2010SW000597.
322 de Soria-Santacruz, M., W. Li, R. M. Thorne, Q. Ma, J. Bortnik, B. Ni, C. A.
323 Kletzing, W. S. Kurth, G. B. Hospodarsky, H. E. Spence, G. D. Reeves, J. B. Blake,
324 and J. F. Fennell (2015), Analysis of plasmaspheric hiss wave amplitudes inferred
325 from low-altitude POES electron data: Technique sensitivity analysis. J. Geophys.
326 Res. Space Physics, 120, 3552–3563. doi: 10.1002/2014JA020941.
327 Elkington, S. R., M. K. Hudson, and A. A. Chan (1999), Acceleration of relativistic
328 electrons via drift-resonant interaction with toroidal-mode Pc-5 ULF
329 oscillations, *Geophys. Res. Lett.*, 26, 3273–3276.
330 Fok, M.-C., R. B. Horne, N. P. Meredith, and S. A. Glauert (2008), Radiation Belt
331 Environment model: Application to space weather nowcasting, *J. Geophys. Res., 113,*
332 A03S08, doi:10.1029/2007JA012558.
333 Friedel, R. H. W., G. D. Reeves, T. Obara (2002), Relativistic electron dynamics in the
334 inner magnetosphere — a review. *J. Atmos. Sol. Terr. Phys*. 64, 265,
335 doi:10.1016/S1364-6826(01)00088-8.
336 Gao, X., W. Li, J. Bortnik, R. M. Thorne, Q. Lu, Q. Ma, X. Tao, and S.
337 Wang (2015), The effect of different solar wind parameters upon significant

338 relativistic electron flux dropouts in the magnetosphere, J. Geophys. Res. Space
339 Physics,120, doi:10.1002/2015JA021182.
340 Horne, R. B., and R. M. Thorne (1998), Potential waves for relativistic electron scattering
341 and stochastic acceleration during magnetic storms, *Geophys. Res. Lett.*, 25(15),
342 3011–3014, doi:10.1029/98GL01002.
343 Horne, R. B., R. M. Thorne, Y. Y. Shprits, N. P. Meredith, S. A. Glauert, A. J. Smith, S.
344 G. Kanekal, D. N. Baker, M. J. Engebretson, J. L. Posch, M. Spasojevic, U. S. Inan, J.
345 S. Pickett, P. M. E. Decreau (2005), Wave acceleration of electrons in the Van Allen
346 radiation belts, *Nature, 437,* 227–230, doi:10.1038/nature03939.
347 Huang, C.-L., H. E. Spence, M. K. Hudson, and S. R. Elkington (2010), Modeling
348 radiation belt radial diffusion in ULF wave fields: 2. Estimating rates of radial
349 diffusion using combined MHD and particle codes, J. Geophys. Res., 115, A06216,
350 doi:10.1029/2009JA014918.
351 Hudson, M. K., Elkington, S. R., Lyon, J. G., Goodrich, C. C. and Rosenberg, T. J.
352 (1999) Simulation of Radiation Belt Dynamics Driven by Solar Wind Variations, in
353 Sun-Earth Plasma Connections (eds J. L. Burch, R. L. Carovillano and S. K.
354 Antiochos), American Geophysical Union, Washington, D. C..
355 doi: 10.1029/GM109p0171.
356 Iles, R. H. A., A. N. Fazakerley, A. D. Johnstone, N. P. Meredith, and P. Bühler
357 (2002), The relativistic electron response in the outer radiation belt during
358 magnetic storms, Ann. Geophys., 20, 957–965, doi:10.5194/angeo-20-957-2002.
359 Jaynes, A. N. et al. (2015), Source and seed populations for relativistic electrons:
360 Their roles in radiation belt changes, J. Geophys. Res. Space Physics, In Press.

361 Kim, H.-J., L. Lyons, V. Pinto, C.-P. Wang, and K.-C. Kim (2015), Revisit of
362 relationship between geosynchronous relativistic electron enhancements and
363 magnetic storms, Geophys. Res. Lett., 42, doi:10.1002/2015GL065192.
364 Li, X., I. Roth, M. Temerin, J. R. Wygant, M. K. Hudson, and J. B.
365 Blake (1993), Simulation of the prompt energization and transport of radiation belt
366 particles during the March 24, 1991 SSC, *Geophys. Res. Lett.*, 20(22),2423–2426.
367 Li, X., M. Temerin, D. N. Baker, G. D. Reeves, and D. Larson (2001), Quantitative
368 prediction of radiation belt electrons at geostationary orbit based on solar wind
369 measurements, Geophys. Res. Lett., 28, 1887.
370 Li, X., D. N. Baker, M. Temerin, G. Reeves, R. Friedel, and C. Shen (2005), Energetic
371 electrons, 50 keV to 6 MeV, at geosynchronous orbit: Their responses to solar wind
372 variations, Space Weather, 3, S04001, doi:10.1029/2004SW000105.
373 Li, W., Y. Y. Shprits, and R. M. Thorne (2007), Dynamic evolution of energetic outer
374 zone electrons due to wave-particle interactions during storms, *J. Geophys. Res., 112*,
375 A10220, doi:10.1029/2007JA012368.
376 Li, W., R. Thorne, J. Bortnik, R. McPherron, Y. Nishimura, V. Angelopoulos, and I. G.
377 Richardson (2012), Evolution of chorus waves and their source electrons during
378 storms driven by corotating interaction regions, *J. Geophys. Res., 117,* A08209,
379 doi:10.1029/2012JA017797.
380 Li, W., B. Ni, R. M. Thorne, J. Bortnik, J. C. Green, C. A. Kletzing, W. S. Kurth, and G.
381 B. Hospodarsky (2013), Constructing the global distribution of chorus wave intensity
382 using measurements of electrons by the POES satellites and waves by the Van Allen
383 Probes, *Geophys. Res. Lett.,* 40,4526–4532, doi:10.1002/grl.50920.

384 Li, W., et al. (2014a), Radiation belt electron acceleration by chorus waves during the 17
385 March 2013 storm, *J. Geophys. Res. Space Physics, 119*, doi:10.1002/2014JA019945.
386 Li, W., B. Ni, R. M. Thorne, J. Bortnik, Y. Nishimura, J. C. Green, C. A. Kletzing, W. S.
387 Kurth, G. B. Hospodarsky, H. E. Spence, G. D. Reeves, J. B. Blake, J. F. Fennell, S.
388 G. Claudepierre, and X. Gu (2014b), Quantifying hiss-driven energetic electron
389 precipitation: A detailed conjunction event analysis, Geophys. Res. Lett., 41, 1085–
390 1092, doi:10.1002/2013GL059132.
391 Lyatsky, W., and G. V. Khazanov (2008), Effect of solar wind density on relativistic
392 electrons at geosynchronous orbit,Geophys. Res. Lett., 35, L03109,
393 doi:10.1029/2007GL032524.
394 McPherron, R. L., D. N. Baker, and N. U. Crooker (2009), Role of the Russell-
395 McPherron effect in the acceleration of relativistic electrons, *J. Atmos. Sol. Terr.*
396 *Phys.*, 71, 1032–1044.
397 Mathie, R. A., and I. R. Mann (2000), A correlation between extended intervals of ULF
398 wave power and storm-time geosynchronous relativistic electron flux
399 enhancements, *Geophys. Res. Lett.*, 27, 3261.
400 Mauk, B. H., N. J. Fox, S. G. Kanekal, R. L. Kessel, D. G. Sibeck, andA. Ukhorskiy
401 (2012), Science Objectives and Rationale for the Radiation Belt Storm Probes
402 Mission, *Space Sci. Rev*., pp. 1–15, doi:10.1007/s11214-012-9908-y.
403 Meredith, N. P., R. B. Horne, M. M. Lam, M. H. Denton, J. E. Borovsky, and J. C. Green
404 (2011), Energetic electron precipitation during high-speed solar wind stream driven
405 storms, *J. Geophys. Res., 116,* A05223, doi:10.1029/2010JA016293.

406 Miyoshi, Y., and R. Kataoka (2008), Flux enhancement of the outer radiation belt
407 electrons after the arrival of stream interaction regions, *J. Geophys. Res.*, 113,
408 A03S09, doi:10.1029/2007JA012506.
409 Ni, B., W. Li, R. M. Thorne, J. Bortnik, J. C. Green, C. A. Kletzing, W. S. Kurth, G. B.
410 Hospodarsky, and M. de Soria-Santacruz Pich (2014), A novel technique to construct
411 the global distribution of whistler mode chorus wave intensity using low-altitude
412 POES electron data, J. Geophys. Res. Space Physics, 119, 5685–5699,
413 doi:10.1002/2014JA019935.
414 Paulikas, G. A., and J. B. Blake (1979), Effects of the solar wind on magnetospheric
415 dynamics: Energetic electrons at the synchronous orbit, in Quantitative Modeling of
416 Magnetospheric Processes, Geophys. Monogr. Ser, vol. 21, edited by W. P. Olson,
417 pp. 180–202, AGU, Washington, D. C.
418 Perry, K. L., M. K. Hudson, and S. R. Elkington (2005), Incorporating spectral
419 characteristics of Pc5 waves into three-dimensional radiation belt modeling and the
420 diffusion of relativistic electrons, *J. Geophys. Res., 110*, A03215,
421 doi:10.1029/2004JA010760.
422 Reeves, G. D., K. L. McAdams, R. H. W. Friedel, and T. P. O'Brien (2003), Acceleration
423 and loss of relativistic electrons during geomagnetic storms, Geophys. Res. Lett., 30,
424 1529, doi:10.1029/2002GL016513, 10.
425 Reeves, G. D., S. K. Morley, R. H. W. Friedel, M. G. Henderson, T. E. Cayton, G.
426 Cunningham, J. B. Blake, R. A. Christensen, and D. Thomsen (2011), On the
427 relationship between relativistic electron flux and solar wind velocity: Paulikas and
428 Blake revisited, J. Geophys. Res., 116, A02213, doi:10.1029/2010JA015735.

429 Reeves, G., et al. (2013) Electron acceleration in the heart of the Van Allen radiation
430 belts, *Science*, doi: 10.1126/science.1237743.
431 Shprits, Y. Y., R. M. Thorne, R. Friedel, G. D. Reeves, J. Fennell, D. N. Baker, and S. G.
432 Kanekal (2006), Outward radial diffusion driven by losses at magnetopause, J.
433 Geophys. Res., 111, A11214, doi:10.1029/2006JA011657.
434 Shue, J.-H., et al. (1998), Magnetopause location under extreme solar wind conditions, J.
435 Geophys. Res., 103(A8), 17691–17700, doi:10.1029/98JA01103.
436 Spence, H. E., et al. (2013), Science goals and overview of the Energetic particle,
437 Composition, and Thermal plasma (ECT) suite on NASA's Radiation Belt Storm
438 Probes (RBSP) mission, *Space Sci. Rev.*, 179, 311–336, doi:10.1007/s11214-013-
439 0007-5.
440 Summers, D., C. Ma, N. P. Meredith, R. B. Horne, R. M. Thorne, D. Heynderickx, and R.
441 R. Anderson (2002), Model of the energization of outer-zone electrons by whistler-
442 mode chorus during the October 9, 1990 geomagnetic storm, *Geophys. Res. Lett.*,
443 *29*(24), 2174, doi:10.1029/2002GL016039.
444 Tao, X., J. M. Albert, and A. A. Chan (2009), Numerical modeling of multidimensional
445 diffusion in the radiation belts using layer methods, J. Geophys. Res., 114, A02215,
446 doi:10.1029/2008JA013826.
447 Thorne, R. M. et al. (2013), Rapid local acceleration of relativistic radiation belt electrons
448 by magnetospheric chorus, *Nature*, *504*, 411-414, doi:10.1038/nature12889.
449 Tu, W., G. S. Cunningham, Y. Chen, S. K. Morley, G. D. Reeves, J. B. Blake, D. N.
450 Baker, and H. Spence (2014), Event-specific chorus wave and electron seed

451 population models in DREAM3D using the Van Allen Probes, *Geophys. Res.*
452 *Lett., 41*, doi:10.1002/2013GL058819.
453 Turner, D. L., Y. Shprits, M. Hartinger, and V. Angelopoulos (2012), Explaining sudden
454 losses of outer radiation belt electrons during geomagnetic storms, Nat. Phys., 8, 208–
455 212, doi:10.1038/Nphys2185.
456 Turner, D. L., et al. (2014), On the cause and extent of outer radiation belt losses during
457 the 30 September 2012 dropout event, J. Geophys. Res. Space Physics, 119, 1530–
458 1540, doi:10.1002/2013JA019446.
459 Ukhorskiy, A. Y., M. I. Sitnov, K. Takahashi, and B. J. Anderson (2009), Radial
460 transport of radiation belt electrons due to stormtime Pc5 waves, *Ann.*
461 *Geophys.*, *27*, 2173–2181.
462 Webb, F., and J. H. Allen (2004), Spacecraft and ground anomalies related to the
463 October-November 2003 solar activity, Space Weather, 2, S03008,
464 doi:10.1029/2004SW000075.
465 Xiao, F., Z. Su, H. Zheng, and S. Wang (2009), Modeling of outer radiation belt electrons
466 by multidimensional diffusion process, *J. Geophys. Res., 114*, A03201,
467 doi:10.1029/2008JA013580.
468 Yuan, C. J., and Q. G. Zong (2013), Relativistic electron fluxes dropout in the outer
469 radiation belt under different solar wind conditions, J. Geophys. Res. Space Physics,
470 118, 7545–7556, doi:10.1002/2013JA019066.
471

472 **Figure captions**

Figure 1. A representative example of an efficient radiation belt electron acceleration event, which occurred during the 8-9 Oct 2012 storm. (a) Solar wind dynamic pressure, (b) solar wind velocity along the x direction, (c) interplanetary magnetic field in z direction in GSM coordinate, (d) SYM-H, and (e) AL. (f-h) Electron fluxes measured by the REPT instrument on Van Allen Probes averaged over each 3-hour bin at three different energy channels. (i) Electron phase space density (PSD) calculated for μ = 3433 MeV/G and K = 0.11 $R_E G^{1/2}$, (j) maximum electron PSD over 2.5-6 R_E (PSD_{max}) in each 3-hour bin. (k) Chorus wave amplitudes averaged over all MLT sectors as a function of L-shell. The vertical magenta line represents the zero epoch time used to perform the superposed epoch analysis.

Figure 2. The same format as Figure 1 but for an example of an inefficient acceleration event.

Figure 3. Superposed epoch analysis results of solar wind parameters, magnetopause location (L_{MP}), geomagnetic indices, and electron and chorus wave evolution for 16 efficient acceleration (EA) events. Superposed epoch analysis results of (a) solar wind dynamic pressure, (b) solar wind velocity, (c) B_z, (d) magnetopause location on the subsolar distance, (e) SYM-H, (f) AL, and (g) PSD_{max}, where the red solid and dashed line represent the mean and median values respectively. (h) Superposed epoch analysis result of chorus wave intensity averaged over all MLT sectors using the POES technique as a function of L-shell. The dashed vertical black line represents the zero epoch time.

Figure 4. The same format as Figure 3 but for the superposed epoch analysis results of 17 inefficient acceleration (IA) events.

Figure 5. Comparison of the superposed epoch analysis results during EA and IA events. (a-g) The same format as Figures 3a-3g, but overplotted for both EA (red) and IA (blue) events in the same panel. (h) Superposed epoch analysis result of chorus wave intensity using the POES technique during EA and (i) IA events.

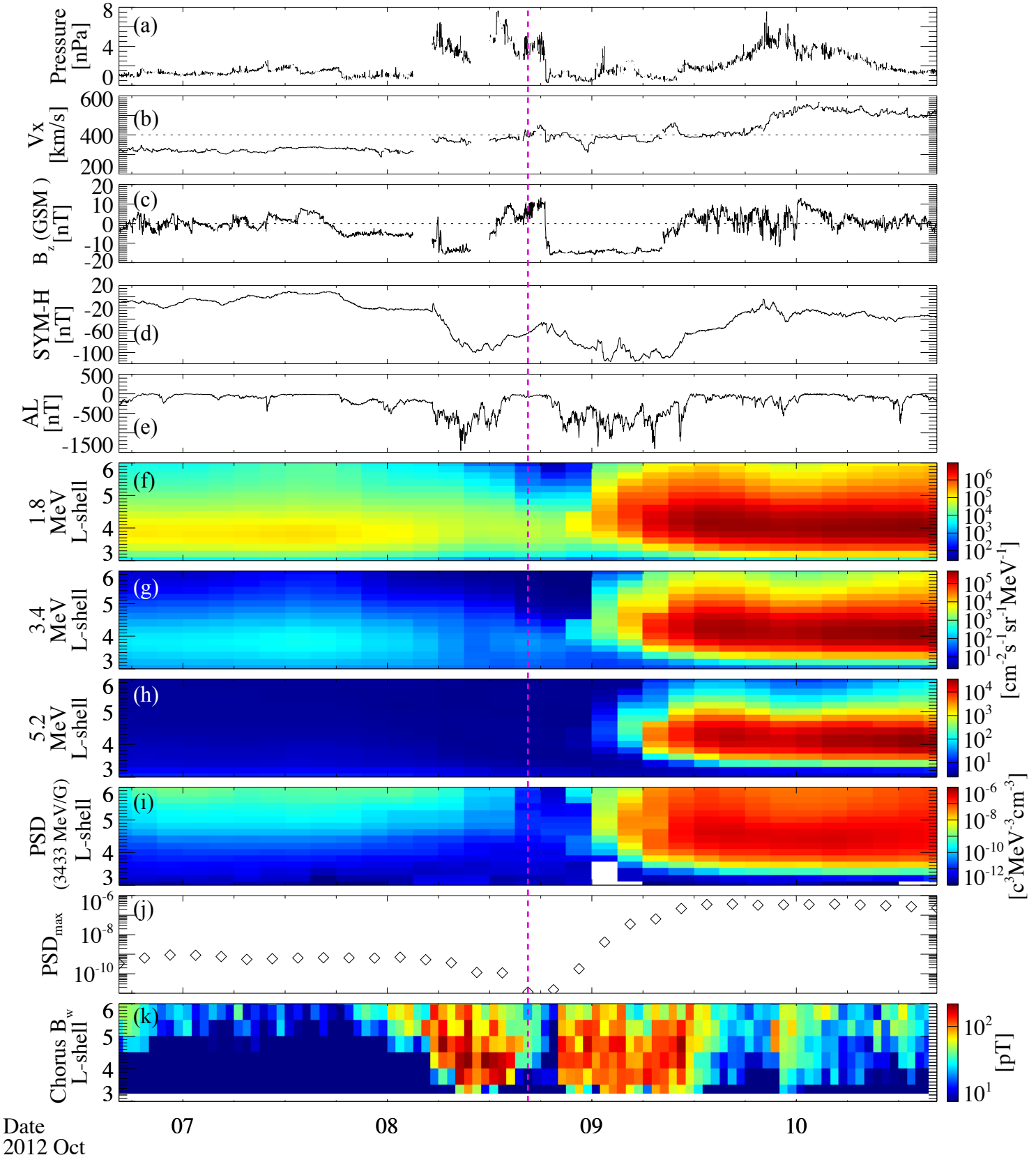
Pressure [nPa]
(a)
Vx [km/s]
(b)
B_z (GSM) [nT]
(c)
SYM-H [nT]
(d)
AL [nT]
(e)
1.8 MeV L-shell
(f)
3.4 MeV L-shell
(g)
5.2 MeV L-shell
(h)
PSD (3433 MeV/G) L-shell
(i)
PSD_max
(j)
Chorus B_w L-shell
(k)
[cm^-2 s^-1 sr^-1 MeV^-1]
[c^3 MeV^-3 cm^-3]
[pT]
Date 2012 Oct
07
08
09
10

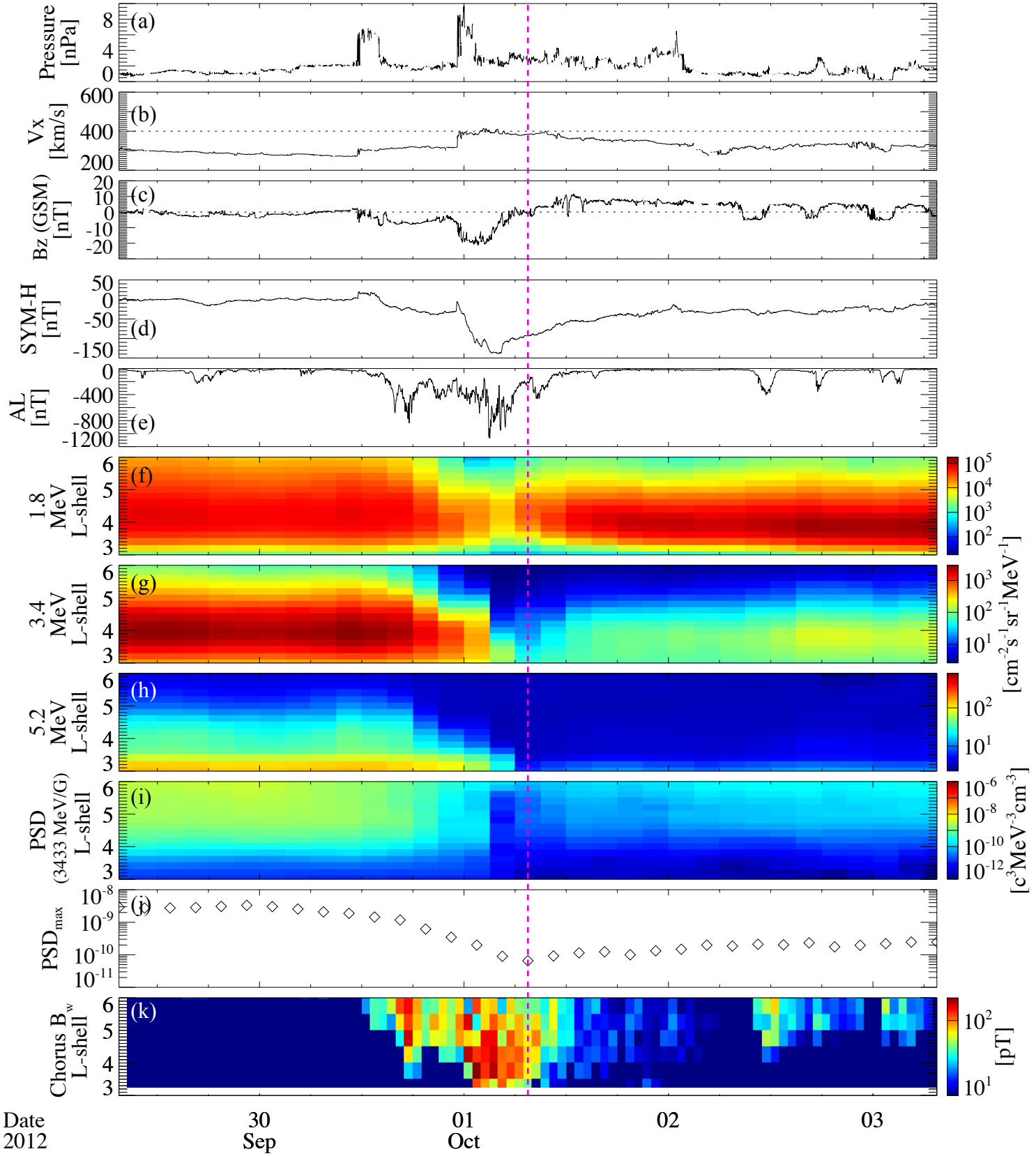
Pressure [nPa]
(a)
Vx [km/s]
(b)
Bz (GSM) [nT]
(c)
SYM-H [nT]
(d)
AL [nT]
(e)
1.8 MeV L-shell
(f)
3.4 MeV L-shell
(g)
5.2 MeV L-shell
(h)
PSD (3433 MeV/G) L-shell
(i)
PSDmax
(j)
Chorus Bw L-shell
(k)
[cm-2s-1sr-1MeV-1]
[c3MeV-3cm-3]
[pT]
Date 2012
30 Sep
01 Oct
02
03

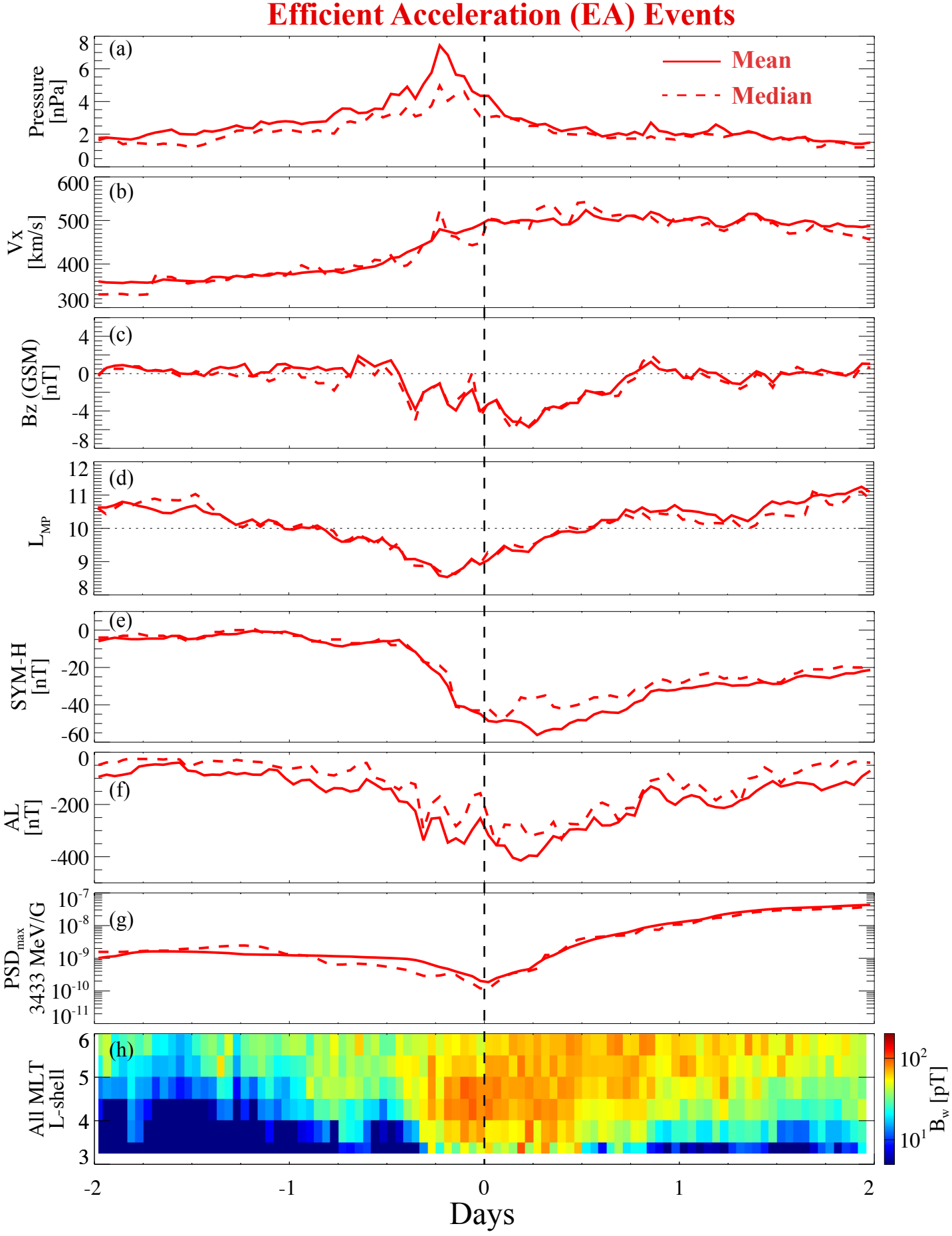
Efficient Acceleration (EA) Events
(a)
Pressure [nPa]
Mean
Median
(b)
Vx [km/s]
(c)
Bz (GSM) [nT]
(d)
L_{MP}
(e)
SYM-H [nT]
(f)
AL [nT]
(g)
PSD_{max} 3433 MeV/G
(h)
All MLT L-shell
B_w [pT]
Days

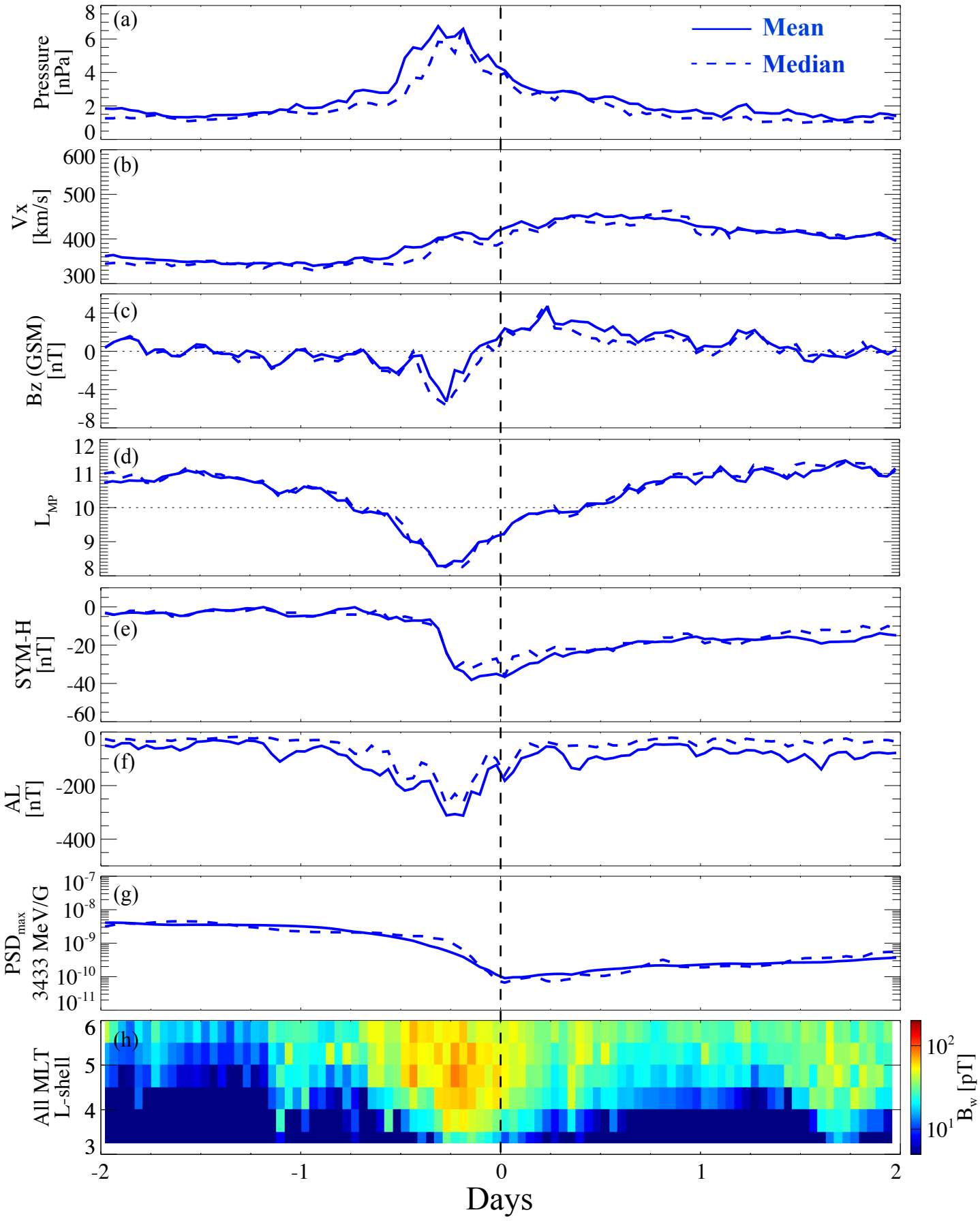
Inefficient Acceleration (IA) Events
(a)
Pressure [nPa]
Mean
Median
(b)
Vx [km/s]
(c)
Bz (GSM) [nT]
(d)
L_{MP}
(e)
SYM-H [nT]
(f)
AL [nT]
(g)
PSD_{max} 3433 MeV/G
(h)
All MLT L-shell
B_w [pT]
Days

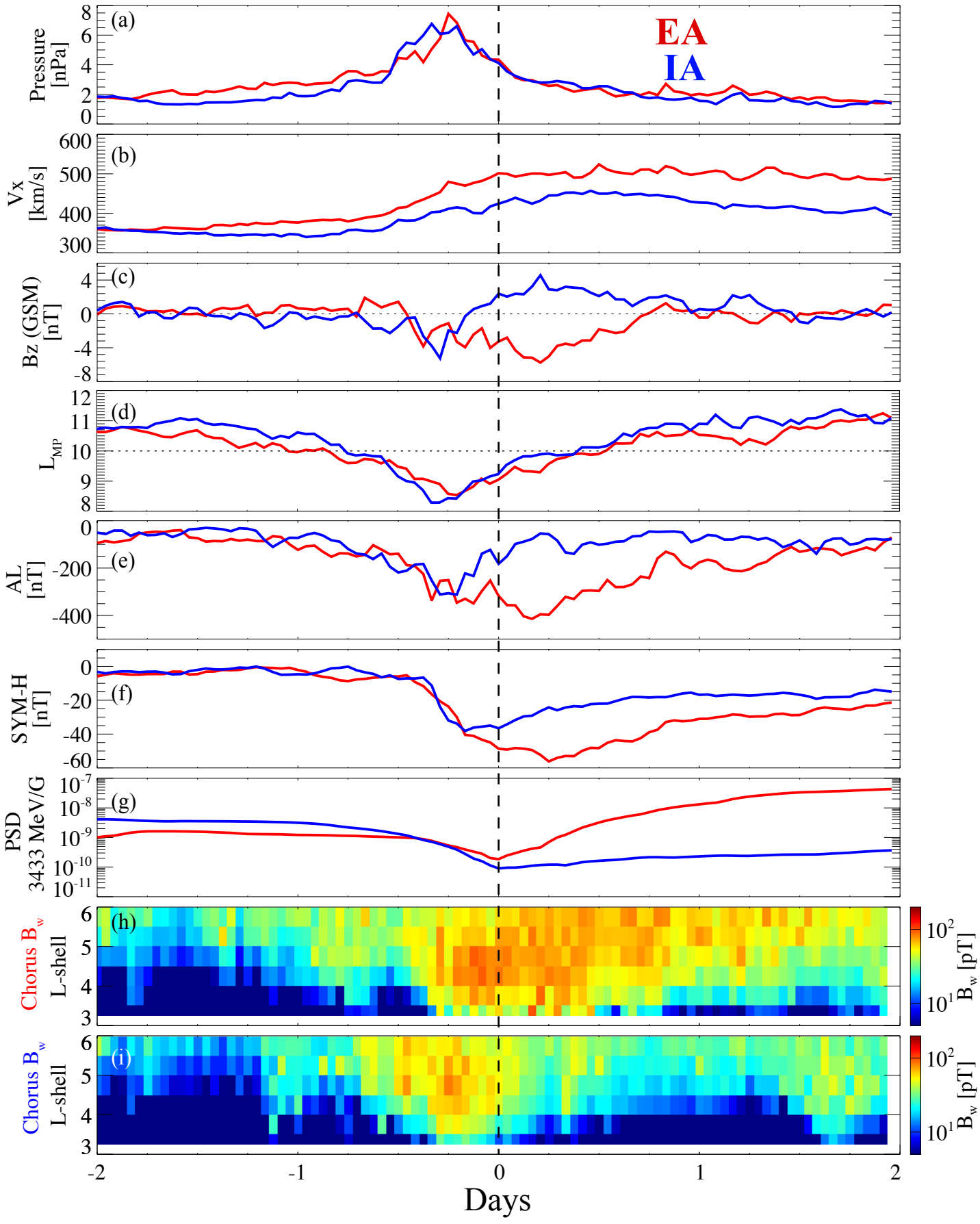
EA
IA
(a)
Pressure [nPa]
(b)
Vx [km/s]
(c)
Bz (GSM) [nT]
(d)
L_{MP}
(e)
AL [nT]
(f)
SYM-H [nT]
(g)
PSD 3433 MeV/G
(h)
Chorus B_w L-shell
(i)
Chorus B_w L-shell
B_w [pT]
Days